NANO LETTERS

Letter

Current-Phase Relationship, Thermal and Quantum Phase Slips in Superconducting Nanowires Made on a Scaffold Created Using Adhesive Tape

Myung-Ho Bae, Robert C. Dinsmore III, Thomas Aref, Matthew Brenner, and Alexey Bezryadin

Nano Lett., **Article ASAP** • DOI: 10.1021/nl803894m • Publication Date (Web): 03 April 2009

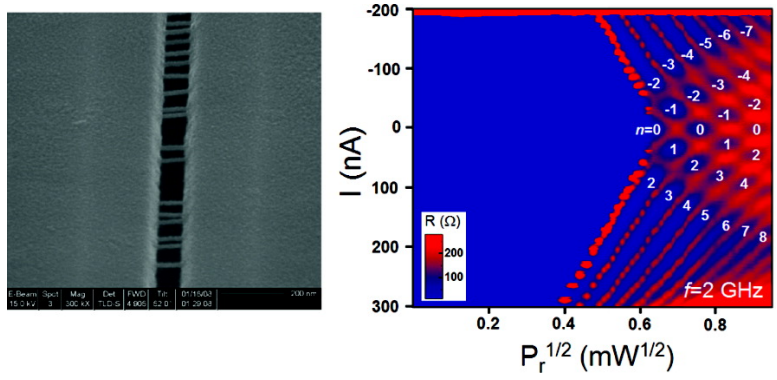

More About This Article

Additional resources and features associated with this article are available within the HTML version:

- Supporting Information
- Access to high resolution figures
- Links to articles and content related to this article
- Copyright permission to reproduce figures and/or text from this article

View the Full Text HTML

Nano Letters is published by the American Chemical Society. 1155 Sixteenth Street N.W., Washington, DC 20036

NANO LETTERS

XXXX
Vol. xx, No. x
-

Current-Phase Relationship, Thermal and Quantum Phase Slips in Superconducting Nanowires Made on a Scaffold Created Using Adhesive Tape

Myung-Ho Bae,* Robert C. Dinsmore III, Thomas Aref, Matthew Brenner, and Alexey Bezryadin

Department of Physics, University of Illinois at Urbana−Champaign, Urbana 61801, Illinois

Received December 24, 2008; Revised Manuscript Received February 22, 2009

ABSTRACT

Quantum phase slippage (QPS) in a superconducting nanowire is a new candidate for developing a quantum bit [Mooij et al. *New J. Phys.* 2005, *7*, 219; Mooij et al. *Nat. Phys.* 2006, *2*, 169; Khlebnikov http://arxiv.org/abs/quant-ph/0210019 2007]. It has also been theoretically predicted that the occurrence of QPS significantly changes the current-phase relationship (CPR) of the wire due to the tunneling between topologically different metastable states [Khlebnikov *Phys. Rev. B* 2008, *78*, 014512]. We present studies on the microwave response of the superconducting nanowires to reveal their CPRs. First, we demonstrate a simple nanowire fabrication technique, based on commercially available adhesive tapes, which allows making thin superconducting wire from different metals. We compare the resistance vs temperature curves of $Mo_{76}Ge_{24}$ and Al nanowires to the classical and quantum models of phase slips. In order to describe the experimentally observed microwave responses of these nanowires, we use the McCumber−Stewart model [McCumber *J. Appl. Phys.* 1968, *39*, 3113; Stewart *Appl. Phys. Lett.* 1968, *12*, 277], which is generalized to include either classical or quantum CPR.

Superconducting nanowires (SNWs) have acquired a lot of attention recently due to their potential application in photon detectors[5] and in quantum bits.[1,2] The fundamental interest in SNWs is motivated by the observation of quantum phase slip (QPS) in them.[6−10] The supercurrent in a SNW is determined by the phase difference ϕ between two ends of the SNW, and the relationship is known as the current-phase relationship (CPR). Although it has been assumed for many decades that CPR of long wires is multivalued,[11,12] recent analysis of this problem that has taken QPS into account has shown that CPR must be single-valued.[3,13] A useful way to probe the CPR is to study the superconducting transport under microwave (MW) radiation,[14] which changes the phase difference periodically and produces lock-in resonances, which occur as voltage plateaus on the voltage−current ($V(I)$) curves, known as Shapiro steps (ShSs).[15,16]

In this letter, we investigate such resonant behaviors in two different wires: $Mo_{76}Ge_{24}$ and Al nanowires. To fabricate these nanowires, we have developed a simple method based on adhesive tape scaffolds. We measure $V(I)$ curves under MWs and observe voltage plateaus on them, which correspond to the phase lock-in resonances. Both $Mo_{76}Ge_{24}$ and Al SNWs show half-integer resonances, at high enough frequencies (above ∼8 GHz). We model this phenomenon using the McCumber−Stewart approach,[4] by assuming a nonsinusoidal CPR. The best agreement between the models and the data is obtained if we assume that transport properties of $Mo_{76}Ge_{24}$ wires are dominated by thermally activated phase slips (TAPS) and long enough to have a multivalued CPR. Yet, at the same time, $R(T)$ curves of $Mo_{76}Ge_{24}$ wires can be fit with theoretical curves originating from QPS theories.[17,18] Thus the possibility of QPS effects influencing $R(T)$ curves cannot be excluded. The Al wire sample also shows fractional Shapiro steps. This fact indicates that the CPR of the wire can not be a nonquantum shortwire limit CPR.[11] We explain the results using quantum CPR due to the work of Khlebnikov.[3,13] Yet, the possibility that the wire is not short enough and thus its CPR is close to the multivalued case (i.e., in the intermediate regime) cannot be excluded definitely.

We observe that when a piece of an adhesive tape is attached to a flat substrate with a trench[19] and subsequently peeled off from the substrate as shown in Figure 1a, some polymer nanostrings are suspended over the trench if the width of the trench is sufficiently small, i.e., a few micrometers wide or less [see also the Supporting Information]. Figure 1b shows a scanning electron microscope (SEM) image of

* Corresponding author. E-mail: mhbae@illinois.edu.

10.1021/nl803894m CCC: $40.75

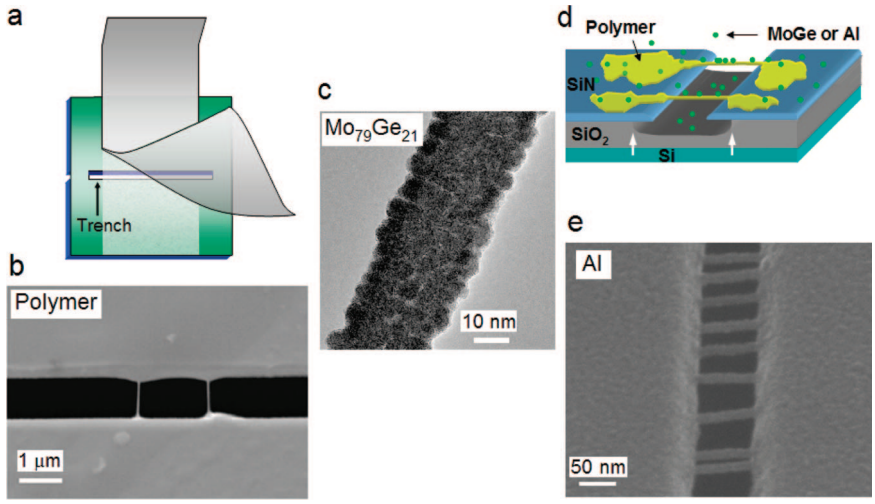

Figure 1. (a) Schematic of a tape-peel-off technique with an adhesive tape on a substrate having a trench, which is prepared as in ref 19. After the peel-off process, some polymer strings are suspended over the trench. (b) Scanning electron microscope (SEM) image of two polymer strings suspended across a trench, where the width and the length of the strings are 45 nm and 0.8 μm, respectively. (c) High-resolution TEM image of a polymer string after a deposition of a 12 nm thick $Mo_{76}Ge_{24}$ film. (d) Schematic of a substrate with an undercut-trench with polymer strings, where arrows indicate undercuts forming in the SiO_2 layer. Metals such as $Mo_{76}Ge_{24}$ and Al (green scattered points) are sputtered on the substrate after the formations of nanostrings over a trench. (e) SEM image with a 52° tilt angle, with the axis of the tilt being perpendicular to the trench and lying in the plane of the sample. Twenty-five nm-thick Al nanowires appear over the trench, produced by a deposition of Al. The width of the trench is 80 nm.

two parallel representative polymer nanostrings suspended over a trench after the "tape-peel-off" process, where the width of the trench is ~1.2 μm. The widths of both strings are ~45 nm. We noticed that narrower trenches gave smaller widths. For example, 20 nm-wide strings have been obtained over an 80-nm-wide trench (Figure 1e).

We sputtered amorphous $Mo_{76}Ge_{24}$ alloy to the substrate having nanostrings under a pressure of 1×10^{-7} Torr at room temperature. Samples for a high-resolution transmission electron microscope (TEM) imaging were prepared by depositing polymer nanostrings on TEM compatible slits as shown in Figure 1a. Figure 1c shows a high-resolution TEM image of part of the 12 nm-thick $Mo_{76}Ge_{24}$ nanowire on a 0.8 μm-long nanostring template, where the width (w) of the nanostring is 28 nm. Figure S1d of the Supporting Information shows the entire TEM image of the nanowire of Figure 1c. Figure S1e of the Supporting Information also shows that the metal connection from a thin film electrode to the nanowire is very smooth. To perform electronic transport measurements, we fabricated an undercut-trench substrate as shown in Figure 1d, where the undercuts forming at the SiO_2 layer are indicated by arrows. After the formation of the nanostrings over the undercut-trench, we used a PDMS (polydimethylsiloxane) contact mask to define thin-film electrodes. Figure 1e shows an SEM image of many Al nanowires in parallel, after sputtering a 25 nm-thick layer of Al metal, where all nanowires show nearly the same width of 20 nm. We cut all nanowires, except one, by a focused ion beam and got a sample with one nanowire across the electrodes as shown in the lower inset of Figure 2a. In the sample preparation process with polymer nanostrings, we did not use any chemical process because polymers can be easily damaged by chemical treatments.

The open and closed red circles of Figure 2a correspond to $R(T)$ curves for two different $Mo_{76}Ge_{24}$ nanowires [MoGe1 (right) length = 150 nm, w = 20 nm; and MoGe2 (left) length = 155 nm, w = 20 nm], respectively. The details of the experimental setup are explained in the Methods section. For MoGe1, $T_{C,film}$ (the critical temperature of the thin film leads connected to the wire) of a 14 nm-thick $Mo_{76}Ge_{24}$ film was 6.2 K. Below $T_{C,film}$, the $R(T)$ curve shows a long flat resistive region, and then, it shows one more superconducting transition in the nanowire at $T_C \sim 4$ K and the resistance goes below our noise level at $T \sim 3$ K.

In a narrow superconducting channel, a resistance below T_C can be due to TAPS.[20−22] A simple approximate semi-phenomenological formula to fit the $R(T)$ curves is the Arrhenius−Little (AL) formula:[23,24]

$$R_{AL}(T) = R_N \exp\left(-\frac{\Delta F(T)}{k_B T}\right) \quad (1)$$

Here $\Delta F(T)[\approx 0.83[\sigma/\xi(0)](R_Q/\rho)k_B T_C(1 - T/T_C)^{3/2}]$ is the energy barrier for phase slips,[21,25] R_Q [$= h/4e^2 = 6.45$ kΩ] is the quantum resistance, k_B is the Boltzmann constant, R_N [$= \rho L/\sigma$] is the normal resistance of the wire, ρ [~ 200 $\mu\Omega$ cm for a MoGe film] is the electric resistivity, σ is the cross section of the wire, and the coherence length $\xi(0)$ is predefined in a dirty limit.[26] The adjustable fitting parameters are T_C, L, and σ. The fitting result using eq 1 is shown by a solid black curve on the $R(T)$ curves of MoGe1 with the fitting parameters: $T_C = 3.73$ K, $\sigma = 250$ nm^2, and $L = 99$ nm. The length of the wire measured under SEM was 150 nm. The coherence length was computed from the T_C and was $\xi(0) = 8.8$ nm. The fitting is consistent with the experimental results. In the case of MoGe2, the best fit is obtained with parameters of $T_C = 2.72$ K, $\sigma = 56$ nm^2, and $L = 57$ nm with $\xi(0) = 10.3$ nm and the actual length of 155 nm. Since the length of $Mo_{76}Ge_{24}$ nanowires is suf-

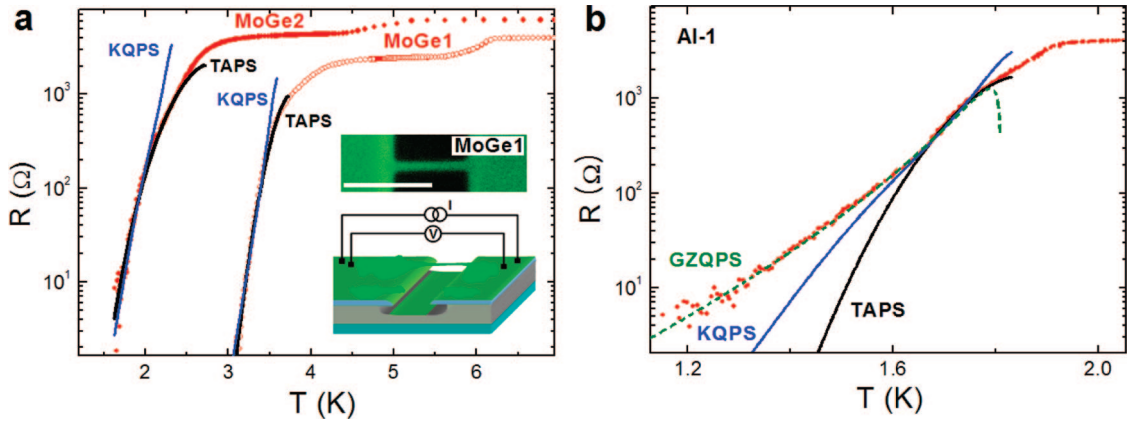

Figure 2. (a) $R(T)$ curves of two $Mo_{76}Ge_{24}$ nanowires (MoGe1, open circles, and MoGe2, closed circles). The solid black line on each $R(T)$ curve is the best fit produced by the Arrhenius−Little (AL) formula $R_{AL}(T)$ (eq 1), which is due to TAPS, with the three fitting parameters listed in the text. The solid blue lines are obtained from the Khlebnikov QPS theory (KQPS), $R_{KQPS}(T)$.[3,13] (upper inset): SEM image of wire MoGe1. The scale bar is 200 nm. (lower inset): Schematic for the transport measurement setup. The lower nanowire, drawn in Figure 1d, is removed. A focused ion beam is used to remove unwanted nanowires. (b) $R(T)$ curve of an Al nanowire (Al-1, scattered points). The dashed green curve is the prediction of the Golubev−Zaikin QPS theory ($R_{GZQPS}(T)$)[28] with five fitting parameters (listed in the text), and the solid black curve corresponds to the phenomenological AL fit ($R_{AL}(T)$).[23] The solid blue line is the best fit predicted by KQPS theory.

ficiently longer than $\xi(0)$ and $\sqrt{\sigma} < 4.4\xi$, these wires are in a quasi-one-dimensional long wire limit.[11,20,21]

On the other hand, the $R(T)$ curve of the Al nanowire [Al-1, length = 80 nm, w = 20 nm; the nominal thickness is 25 nm] in Figure 2b shows a long resistance tail, occurring at $T < T_{C,film}$. The AL fit (a black curve) shows a deviation from data below T = 1.62 K because the measured tail has a positive curvature. The AL fit always has a negative curvature (in the log-linear plot) because the thermal activation is governed by Arrhenius-type exponential term, like in Figure 2a. In addition, the coherence length 3.5 nm estimated from the TAPS fitting (i.e., using the AL fit) is much shorter than the computed length of (50 ± 20) nm in a dirty limit with ξ_0 = 1.6 μm and l = (2 ± 1) nm for a ∼25 nm thick Al film.[27] Following previous experiments on Al wires,[10] we attempt to explain the results using a notion of QPS. In these events the phase slips by 2π through a QPS process. The $R(T)$ curve, considering the dissipation by QPS in the Golubev−Zaikin (GZ) theory,[28,10] is

$$R_{GZQPS}(T) = BR_Q S_{QPS}(L/\xi(T)) \exp[-S_{QPS}] \qquad (2)$$

where S_{QPS} [$= A(R_Q/R_N)(L/\xi(T))$] is the effective action and B and A are adjustable parameters. The dashed green curve in Figure 2b is the best fit to eq 2, with $\xi(0)$ = 60 nm, where the adjustable parameters were T_C = 1.81 K, R_N = 1.37 kΩ, L = 80 nm, B = 5.1, and A = 3. Note that in this case we fit the data using only the QPS term, without including the TAPS term.[10] The Al-1 fit in Figure 2b is in good agreement with the data, which indicates that the resistance tail could originate from the QPS. Now we compare our results to the experiment of Zgirski et al.[29] Their $R(T)$ measurements show that homogeneous wires which are thinner than ∼15 nm in diameter can show a pronounced QPS behavior. Homogeneous wires which are thicker than that, say ∼17 nm in diameter, show only signatures of thermally activated phase slips. Yet non-Arrhenius tails can be observed quite frequently in as-produced Al wires, even in those which have comparatively large diameter of e.g. ∼70 nm. Clearly such tails are due to weak links, the presence of which greatly increases the probability of TAPS and possibly QPS.

Since our wire is ∼20−25 nm in diameter, most probably the tail we observe is due to some narrow spot in the wire. Yet this narrow segment itself constitutes a weak link which can be analyzed in order to determine whether its resistance is due to TAPS or QPS. On the other hand, since a resistance tail can also originate from external noise or the inhomogeneity of the nanowire,[30] one should be careful in the analysis with $R(T)$ curves.

Recently, some theories have predicted that superconducting wires in the QPS regime can show a sharp (Arrhenius-type) decrease of the resistance with decreasing temperature.[17,18] We compare the experimental $R(T)$ curves to such a theory. It was developed by Khlebnikov,[18] and it is valid when the QPS rate is low. The resistance as a function of temperature is given by $R_{KQPS}(T) = R_N \exp[-(\pi^2 R_Q \Delta(T))/(4R_N T) \tanh(\Delta(T)/2T)]$,[18] where $\Delta(T)$ is the BCS (Bardeen−Cooper−Schrieffer) superconducting gap energy. The fits are shown by sold blue lines in Figure 2. The best fitting parameters were T_C = 3.6 K and R_N = 1.7 kΩ for MoGe1, T_C = 2.32 K and R_N = 3.6 kΩ for MoGe2, and T_C = 1.83 K and R_N = 3.2 kΩ for Al-1. The fits agree well with the MoGe wire data but not with the Al wire data, probably due to a high fugacity of QPS in our Al sample or the presence of weak links. Now we discuss MoGe samples. The measured values for the normal resistance were R_N = 2.5 and 4.3 kΩ for MoGe1 and MoGe2, respectively. Thus we find that R_N used in the KQPS fits is in approximate agreement (same order of magnitude) with the measured R_N. These fits, as well as those done by Meiden et al.,[17] suggest a possibility that QPS (possibly thermally assisted QPS), not TAPS, explain the resistance of nanowires at temperatures

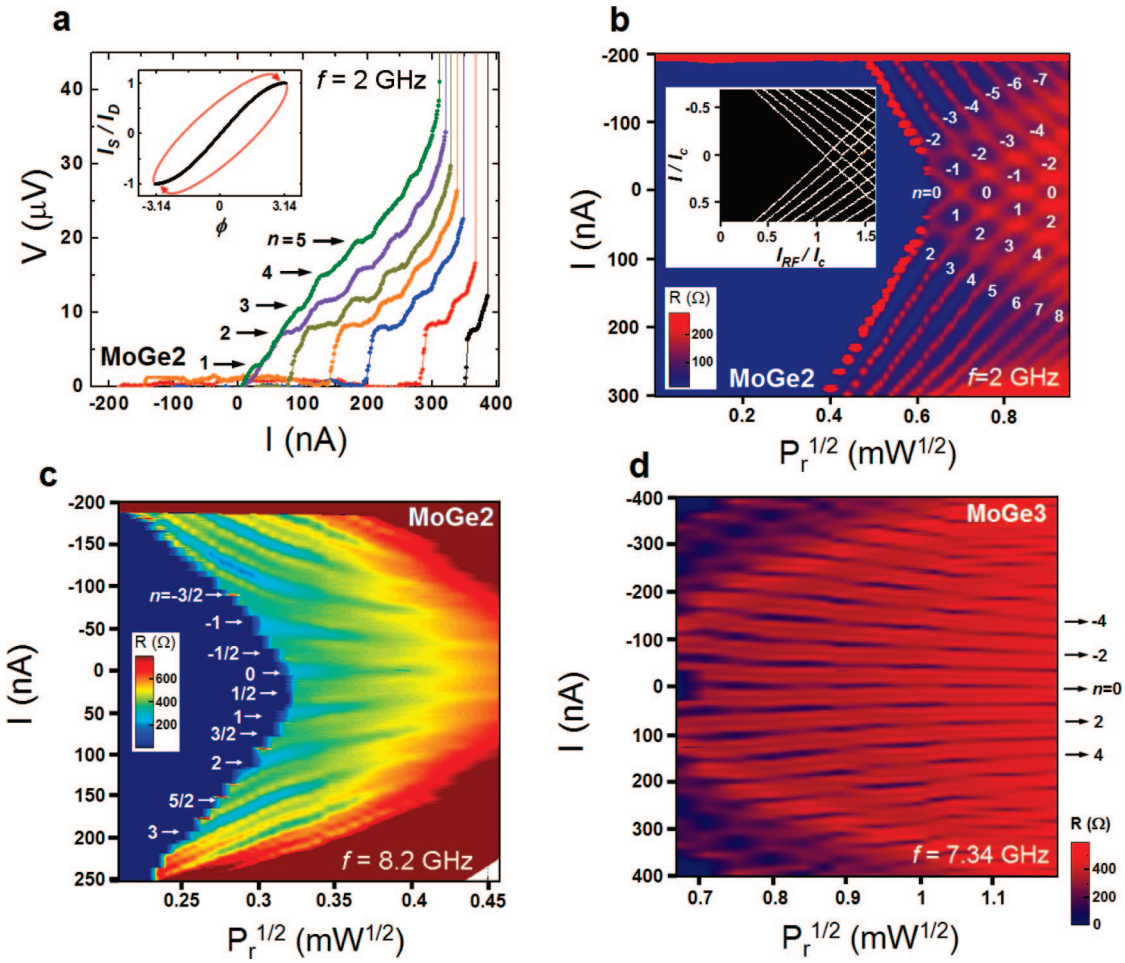

Figure 3. (a) $V(I)$ curves of the sample MoGe2 under external MWs of frequency $f = 2$ GHz at output power $P = -9.5$, -8, -6.5, -5.6, -4.8, -4, and -3 dBm, from the right to the left, measured at $T = 0.32$ K. The arrows indicate the quantized voltage corresponding to multiple integers of the quantum $hf/2e = 4.1\ \mu$V. (inset): Example plot of the LY multivalued CPR[11,12] (note that only one branch is shown) for a nanowire with $L/\xi(T) = 5.6$ (for $T = 0.32$ K), where red arrows indicate phase slip phenomena (see text). (b) $dV/dI(I, P_r^{1/2})$ plot for the sample MoGe2, measured at $T = 0.32$ K and $f = 2$ GHz. The large blue-colored region on the left is the supercurrent region. The Shapiro plateaus are also blue, since they are close to being horizontal. They are indicated by index integer numbers. (inset): $dV/dI(I/I_C, I_{RF}/I_C)$ plot, which was calculated with using LY CPR (an example is shown in the inset of part a), where white colored regions correspond to the differential resistance sharp peaks. (c) $dV/dI(I, P_r^{1/2})$ plot for the sample MoGe2 measured at a higher MW frequency, namely at $f = 8.2$ GHz and $T = 0.32$ K. (d) $dV/dI(I, P_r^{1/2})$ plot of a carbon nanotube-templated nanowire (MoGe3) under MW of $f = 7.34$ GHz at $T = 0.32$ K.

comparable to T_C. But, since the AL fit works also quite well, the possibility of TAPS being the dominant phenomenon cannot be ruled out. Qualitatively different experiments, therefore, are needed to establish whether the TAPS or the QPS is the main contributor to the measured resistance. Below we describe one such experiment, which involves microwave radiation.

Figure 3a shows $V(I)$ curves of the sample MoGe2, measured at frequency of $f = 2$ GHz with various nonzero powers of the applied MW at $T = 0.32$ K. Each curve exhibits a resistive branch, induced by the MW. We suggest that the observed resistive state is not simply a normal spot on the wire but a coherent dynamic superconducting state, i.e. a microwave-induced phase-slip center (MW-PSC). This suggestion is confirmed by the observation of ShSs (Figure 3a), which represent a phase lock-in effect, which is possible only if the resistive state is phase coherent. The arrows in Figure 3a are positioned at integer multiples of the microwave photon energy, i.e. at $V_n = nhf/2e$ ($= n \times 4.1\ \mu$V at $f = 2$ GHz),[31] as expected for ShSs. We find that that the position of arrows matches the position of the voltage plateaus, thus confirming that the resistive state, stabilized by MW in our experiment, is phase coherent. The steps occur as downward peaks in the differential resistance (see Figure S2 in the Supporting Information). These peaks represent phase lock-in resonances occurring when the frequency of the revolving superconducting order parameter in the PSC equals an integer multiple of the frequency of the applied MW. Now we consider the current width (ΔI) of the observed steps. Consider for example the second step on the $V(I)$ curve, which appears at $V \approx 8.2\ \mu$V. As the MW power is increased, the step first becomes wider but then narrows again and disappears at $P = -3$ dBm (P is defined as the output power of our MW source). Such oscillatory behavior is observed in almost all steps. This trend is even clearer in a $dV/dI(I, P_r^{1/2})$ plot of Figure 3b, where P_r is the output MW power expressed in milliwatt units as $P_r = 10^{P[\mathrm{dBm}]/10}$ mW. Such plateaus appear as minima (blue color) in the plot and exhibit pronounced

"diamond" structures. Each diamond is marked with an integer number, corresponding to the order of the resonance. The presence of the diamond structure shows explicitly the quasi-periodic oscillation of the current widths of the voltage plateaus in the corresponding $V(I)$ curves (Figure 3a).

Now, we suggest a model to describe the data of the type shown in Figure 3b. In a long wire limit, Likharev and Yakobson (LY) predicted that the CPR of the nanowire becomes multivalued at $L/\xi(T) \geq 3.6$.[11,12,32] Such LY CPR has a form of $I_S(\phi) = I_C(\phi\xi(T)/L_S)[1 - (\phi\xi(T)/L_S)^2]$, which is illustrated in the inset of Figure 3a (a black solid curve) for the MoGe2 wire with $L/\xi(0.3\text{ K}) \sim 5.6$ for $-3.23 \leq \phi \leq 3.23$, which has a multivalued CPR, and $\xi(T) = \xi(0)(1 - T/T_C)^{-1/2}$. In the LY CPR exemplified in Figure 3a, the phase slip by $+2\pi$ must occur at $\phi_m = 3.23$, for a forward current sweep direction, and at $\phi_m = -3.23$ (by -2π), for a backward current sweep direction, where the ϕ_m points correspond to the maximum supercurrent. The phase slip processes are indicated by red arrows in the inset of Figure 3a. Using this CPR for the phase slip events, we numerically calculated the differential resistance of the wire as a function of a DC current and an AC current ($dV/dI(I/I_C, I_{RF}/I_C)$), using the McCumber−Stewart mode[4] at a reduced frequency $\Omega = 0.08$ in a resistively shunted case [see the Methods section], where I_{RF} is proportional to $P_r^{1/2}$. The result is shown in the inset of Figure 3b. It is qualitatively consistent with experimental results in the main panel of Figure 3b.

With increasing frequency, dV/dI vs $2eV/hf$ (differential conductance vs normalized voltage) curves start to show half-integer steps at $f = 8.2$ GHz as shown in Figure S2a of the Supporting Information.[33] Figure 3c shows the $dV/dI(I, P_r^{1/2})$ plot measured at $f = 8.2$ GHz on MoGe2 at $T = 0.32$ K, where half-integer steps with integer steps are shown. At this high frequency, we observe a new feature: cyan-colored areas surrounding the yellow regions, which correspond to the voltage plateaus and do not cross and there is no diamonds structure. The oscillation amplitude of ΔI (ΔI is the vertical height of a cyan-colored region in Figure 3c, at a fixed power value) with increasing power is also very weak or absent. To check whether these observations are consistent with the multivalued LY CPR in a long wire limit, we numerically calculated $dV/dI(I/I_C, I_{RF}/I_C)$ plots corresponding to three different situations: a short wire case with $L/\xi(0) \ll 1$ (using a single-valued nonsinusoidal CPR suggested by Kulik and Omelyanchuk;[34] Figure S3a) and two long wire cases (multivalued nonsinusoidal LY CPRs) of $L/\xi(0) = 5.6$ (Figure S3b) and $L/\xi(0) = 5.9$ (Figure S3c) at $\Omega = 0.8$ in the Supporting Information. The frequency Ω was tuned to match the apparent highest order of fractional resonances in the data (Figure 3c and d). In the calculation, the current widths corresponding to each voltage plateau in the three cases considered above oscillate with power but do not go to zero at any power. Therefore, this nonzero behavior in ΔI is a common property of these nonsinusoidal CPRs (we checked explicitly that ΔI does go to zero at certain values of the MW power if the CPR is sinusoidal). In the simulation, δI_{min}, the minimum of the current width corresponding to the interval between two resistance peaks for the $n = 0$ Shapiro steps, gets larger with increasing L/ξ (see Figure S3c). Thus, the apparent nonzero δI_{min} with increasing power by $P_r^{1/2} = 0.4\text{ mW}^{1/2}$ in Figure 3c could be related to this multivalued CPR. However, in Figure 3c, the oscillation behavior, predicted by computations (Figure S3c), is not visible. Our explanation is that the examined power is too strong to show a pronounced oscillation behavior, i.e., this system goes to a noncoherent resistive state without resonance steps just above $P_r^{1/2} \sim 0.45\text{ mW}^{1/2}$. To verify that $\Delta I(P)$ can show oscillations with increasing power (as our numerical simulation predicts), we prepared another long wire (MoGe3) using a different method, namely the fluorinated-carbon-nanotube-templating method.[19] The MoGe3 sample was also made of $Mo_{76}Ge_{24}$ alloy. The length of the wire was ~100 nm. Figure 3d shows MWs response ($f = 7.34$ GHz) of the MoGe3. The plot is rich in details. The blue color represents the minima of the differential resistance, i.e. corresponds to various orders of lock-in resonances. In particular, half-integer steps are visible as thin blue lines between the thick blue lines corresponding to integer resonances. Most importantly, the width of the integer ShS remains larger than zero for all measured powers, manifested by the fact that the corresponding blue lines do not exhibit interruptions. The ΔI in current steps corresponding to $n = 0$, 1, 2, and 3 shows weak oscillation behavior with increasing power (as is observed in Figure 3d), which is consistent with calculations in Figure S3c computed for a multivalued CPR in a long wire limit. Thus, we obtain evidence that the QPS rate in MoGe wires is low enough so that CPR remains multivalued, i.e. the QPS rate is much smaller than the applied MW frequency.

Now we consider MW response on Al wire (Al-1). With increasing frequency, dV/dI vs $2eV/hf$ (differential conductance vs normalized voltage) curves start to show half-integer steps near $f = 8.4$ GHz as shown in Figure S2b of the Supporting Information. Figure 4a shows $V(I)$ curves of Al-1 without ($-\infty$ dBm) and with MW radiation of various powers ($f = 8.4$ GHz, $T = 0.6$ K). Under MWs, the $V(I)$ curves show voltage plateaus (indicated by arrows in Figure 4a). The voltage spacing between neighboring voltage plateaus is about $\Delta V = 17.3\ \mu$V, which is consistent with the expected $\Delta V = hf/2e = 17.37\ \mu$V. In addition to integer ShSs, half-integer ShSs ($n = 1/2$, 3/2, 5/2) are also distinguishable in Figure 4a. Figure 4b shows $dV/dI(I, P_r^{1/2})$ at the same frequency. The dark green regions indicated by integer numbers in the plot correspond to the voltage plateaus in Figure 4a.

In Figure 4b, the local minimum resistance regions between two integer ShSs correspond to half-integer ShSs, e.g., the local minimum resistance regions in blue and red dashed closed loops in the plot correspond to $n = 1/2$ and 3/2 half-integer ShSs, respectively. If we consider the temperature dependence of coherence length, we get $\xi = 73$ nm at $T = 0.6$ K with $\xi(0) = 60$ nm. This is nearly the same as the wire length of 80 nm. In what follows we will first compare the results with a nonquantum CPR derived for short limit wires and then with a quantum CPR.

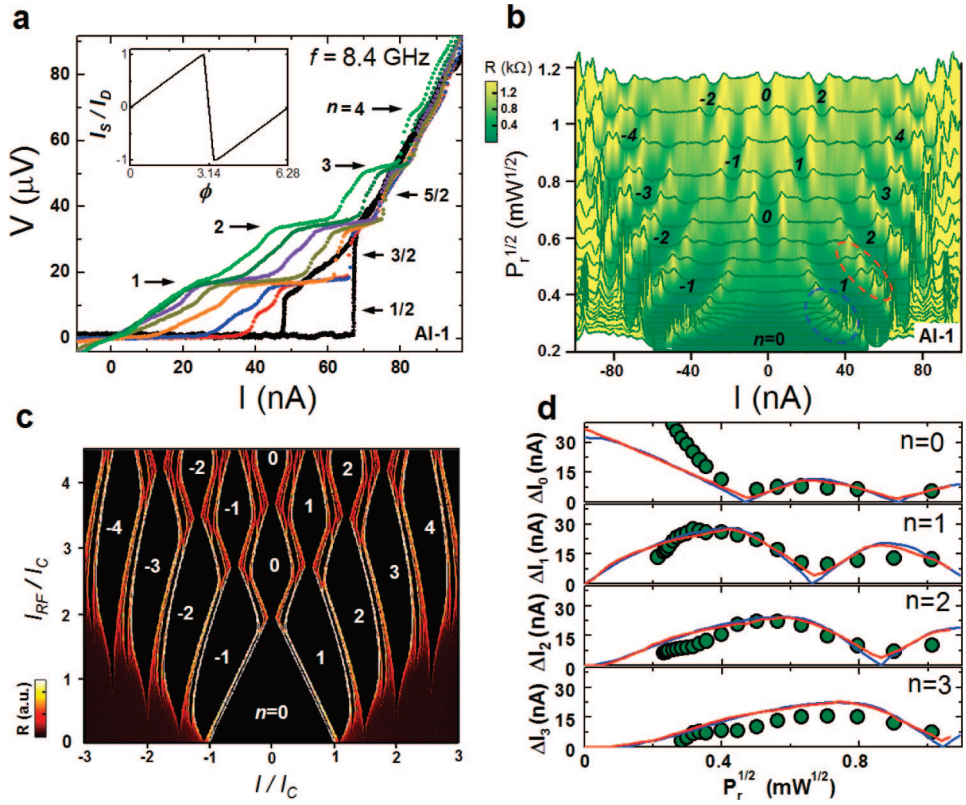

Figure 4. (a) $V(I)$ curves of Al-1 under an external MW of $f = 8.4$ GHz at $P = -\infty$, -11.8, -11, -9.5, -8, -7, -6, and -5 dBm from right to left at $T = 0.6$ K. The MW application induces voltage plateaus in $V(I)$ curves. Arrows with integer index numbers ($n = 1$, 2, 3, and 4) indicate voltage positions predicted by the AC Josephson relation, which match with the positions of the observed voltage plateaus. Half-integer Shapiro steps ($n = 1/2$, 3/2, 5/2) are also visible. (inset) Example plot of a QPS-wire theoretical CPR (see text). (b) Differential resistance as a function of a bias current and power, $dV/dI(I, P_r^{1/2})$ plotted for the Al wire, for $f = 8.4$ GHz at $T = 0.6$ K. Solid curves are raw data. The color-coding represents the interpolation of the data shown by the solid curves. The regions shown by dashed blue and red curves indicate examples of half-integer ShS ($n = 1/2$ for blue and $n = 3/2$ for red). (c) $dV/dI(I/I_C, I_{RF}/I_C)$ plot, numerically calculated by the McCumber−Stewart model, with Khlebnikov quantum theoretical CPR (plotted in the inset of a; also, see the Supporting Information). The integer numbers are index numbers of integer ShS. (d) Closed circles represent current width of voltage plateaus as a function of $P_r^{1/2}$ obtained from b. The red curves are obtained by numerical calculations of c, and the blue curves are obtained from Figure S4 (corresponding to classical short-wire CPR, $I_S^{SW}(\phi)$[11,35]) for $n = 0$,1, 2, and 3.

In the case of $T_C \sim T_{C,film}$, we can use the Likharev nonquantum (LNQ) short-wire CPR[11,35] as $I_S^{SW} = I_C\{[1 + 1/15(L/\xi(T))^2] \sin \phi - 1/30(L/\xi(T))^2 \sin 2\phi\}$. An example of this CPR is plotted in the inset of Figure S4 of the Supporting Information for $L/\xi = 1.09$. It shows only a slight deviation from the sinusoidal CPR. Figure S4 shows a numerically calculated $dV/dI(I/I_C, I_{RF}/I_C)$ based on the LNQ CPR at $\Omega = 0.6$. The current width, ΔI, of the ShS as a function of $P_r^{1/2}$ obtained from Figure S4 (blue curves) is similar to the experimental result (closed circles) as is shown in Figure 4d.[36] On the other hand, no half-integer ShSs have been found in the calculation (Figure S4). Yet, the experiment shows a pronounced half-integer ShSs in Figure 4a and b. Thus, we suggest that LNQ CPR does not apply to our Al wires. Therefore we consider the possibility that QPS is responsible for some observed features. In particular, a resistance tail in Figure 2b suggests existence of QPS in the Al SNW. To incorporate the effect of QPS in the CPR, we use Klebnikov quantum theoretical CPR (KQT CPR) for a QPS-dominated wire, based on the theory of refs 3 and 13, $I_S = (I_C\phi/\pi) - (2\alpha^2/4\pi^3 I_C)(\phi/[1 - (\phi/\pi)^2]^2)$ for $-\pi < \phi < \pi$, where α represents the bare QPS fugacity, which is much smaller than unity (also see the Supporting Information). The inset of Figure 4a shows an example of KQT CPR with $\alpha = 0.1I_C$, which looks like a sawtooth. If α is increased, the CPR becomes closer to the sinusoidal one. Figure 4c shows a numerically calculated $dV/dI(I/I_C, I_{RF}/I_C)$ at $\Omega = 0.6$ based on the quantum KQT CPR. The frequency value of Ω is chosen to make the ratio of the fractional ShS to the integer ShS to be about the same as in the experiment (Figure 4b). Here, the value of α is also chosen to make the ratio ΔI close to the experimental values. The dark regions indicated by integer numbers in the plot correspond to voltage plateaus of integer ShSs. In the simulation (Figure 4c), half-integer ShSs appear as regions of local minima of the differential resistance (black color), between two neighboring integer steps. The origin of the half-integer ShS is the nonsinusoidal, roughly sawtooth shape of the quantum CPR. It is consistent with the half-integer ShSs observed in the experiments as shown in Figures 4a and b. The consistency is also manifested in their ΔI as a function of $P_r^{1/2}$ plots in Figure 4d. A generally good agreement between the theory and experiment is found except for the case of $n = 0$, due to low rates of switching from the static superconducting regime to the dynamic regime. On the other hand, the possibility that the wire is not short enough, i. g., in a case of $\xi(0) \approx$

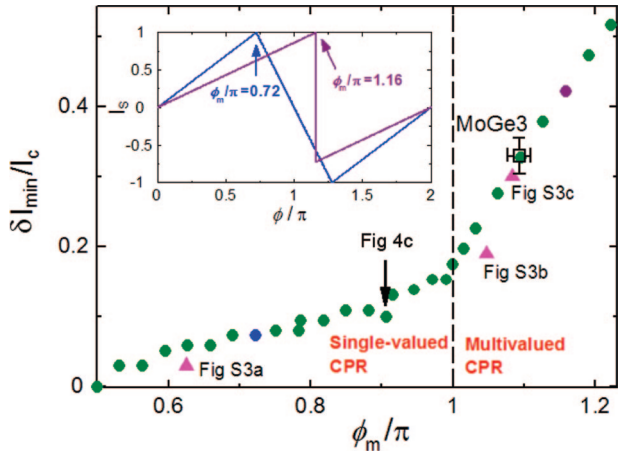

Figure 5. (scattered solid circles) $\delta I_{min}/I_C$ vs ϕ_m, which is obtained by the numerical calculations with various nonsinusoidal CPRs, for example, as shown in the inset, where ϕ_m is the phase value corresponding to the critical current in their current vs phase plots. (solid triangles) Obtained by the numerical calculations based on Figure S3 in the Supporting Information. (inset) Example plots of the nonsinusoidal CPRs, where plots corresponding to $\phi_m = 0.72$ and 1.16 represent a single-valued CPR and multivalued CPR, respectively.

30 nm with $l \approx 1$ nm and $L = 80$ nm, and thus, its CPR being close to the multivalued (i.e., in the intermediate regime) case cannot be excluded definitely. In addition, since the comparison was done with only one sample for each regime, further experimental evidence is needed.

Since both cases of single-valued (see Figure 4c) and multivalued CPRs (see Figure S3 in the Supporting Information) show the nonzero δI_{min}, we plot $\delta I_{min}/I_C$ vs ϕ_m by scattered solid circles in Figure 5 to compare the amplitude of δI_{min} with various CPRs in a simplified model version, for example, as shown in the inset of Figure 5. We found that the normalized δI_{min} increases faster when ϕ_m is larger than π, at which the system enters the regime of the multivalued CPR (the CPR is single-valued for $\phi_m < \pi$). The solid triangles are obtained from Figure S3 based on exact theories for the CPR (as opposed to our model CPR shown in the insert of Figure 5), which also shows a similar trend with the results based on the simplified model CPRs. In Figure 5, an open square with error bars was obtained from MoGe3 (with $I_C \sim 50$ nA estimated from Figure 2d), corresponding to $\delta I_{min}/I_C \sim 0.33$. The position of this open square corresponds to the multivalued CPR regime. This suggests that the resistance in the MoGe3 could originate from TAPS. For the Klebnikov QPS theoretical CPR plotted in the inset of Figure 4a, $\delta I_{min}/I_C \sim 0.1$ was obtained using by Figure 4c, which is indicated by an arrow in Figure 5. In the case of Al SNW, since the noise level in dV/dI values was nearly the same a resistance dip between two peaks for δI_{min} (not shown), it was difficult to define the value of δI_{min}. However, we believe that further precise experiments with sufficiently long wires under MWs could reveal the existence of QPS in SNWs, by using the type of analysis presented here.

In summary, we describe a fabrication method to prepare $Mo_{76}Ge_{24}$ and Al nanowires using adhesive tapes on a substrate with an ~100 nm wide trench. The widths of the nanowires suspended on the ~100 nm-wide trench are regularly ~20 nm. In the case of the $Mo_{76}Ge_{24}$ nanowires, the phase-slip branch under MWs with a relatively high frequency shows pronounced voltage plateaus corresponding to integer and half-integer ShSs, where power dependence of the width of integer ShSs is explained by the multivalued nonsinusoidal CPR in a TAPS-dominated wire. In particular we observe the step width does not go to zero on any MW power, which indicates that the CPR is multivalued. Klhebnikov theory of QPS indicated that if QPS is present then the CPR should be single-valued. Thus, we obtain evidence that QPS is not present in the MoGe wires in the studied regime. The Al wire under MWs also shows integer ShSs with half-integer ShSs. We model the observed width using Khlebnikov quantum CPR, which is expected in the QPS-dominated wire, although no direct proof of QPS is found.

Methods. ***Low-Noise Measurement Setup.*** The transport measurements were performed in four-terminal film-involving configurations in a He^3 cryostat with the base temperature of 0.28 K. Copper powder-filled epoxy and silver-paste glue at cryogenic temperatures and π-filtering system at room temperature are used to suppress the high-frequency noise. All the voltage measurements were done with battery powered preamplifiers (PAR113 and SR560). To measure $R(T)$ curves, we have used a low-frequency bias current with the amplitude of ~10 nA and the frequency of 11 Hz and obtained zero-bias dV/dI by fitting a straight line to the linear region of the $V(I)$ curve. The microwave signal was introduced through a semirigid coaxial cable, with two attenuators placed at 1 K-pot and a copper-helix antenna, which was placed in front of the sample in a Faraday cage and was of the order of 10 mm in size.

McCumber-Stewart Model Applied for Nanowires. As the phase slip center (PSC) develops in the wire, some nonzero normal current can flow through the wire. Thus, the resistively shunted junction model of McCumber and Stewart can be applied.[4] In this case the phase of the superconducting order parameter can be approximately described by the following phase-evolution equation, $d\phi/d\tau + I_S(\phi) = I_{DC} + I_{RF}\sin(\Omega\tau)$, where ϕ is a phase difference between two superconducting electrodes, τ [$= 2\pi f_c t$] is a dimensionless time variable, Ω [$= f/f_C$] is the normalized frequency by the characteristic frequency $f_C = 2eI_CR/h$, R is the resistance of the resistive branch occurring as a result of PSC, and I_{DC} and I_{RF} are dc bias current and ac bias current induced by an external MW normalized by I_C. Thus the fitting parameters is Ω and the MW-induced ac-component of the bias current I_{RF} and the dc bias current are running parameters in the numerical simulations. Here, a supercurrent, $I_S(\phi)$ is determined by a CPR of an examined wire, which depends on its physical property as well as the length scale of a wire, as explained in the main text.

Acknowledgment. The authors appreciate valuable discussion with S. Khlebnikov, J.-S. Ku, and M. Sahu. This work was supported by DOE Grants No. DEFG02-07ER46453. We acknowledge the access to the fabrication facilities at the Frederick Seitz Materials Research Labora-

tory. This work was also partially supported by the Korea Research Foundation Grants No. KRF-2006-352-C00020.

Supporting Information Available: Figures S1−S4 and description of the current-phase relation from the Mathieu equation in a QPS-dominated superconducting wire. This material is available free of charge via the Internet at http://pubs.acs.org.

References

(1) (a) Mooij, J. E.; Harmans, C. J. P. *New J. Phys.* **2005**, *7*, 219. (b) Mooij, J. E.; Nazarov, Y. V. *Nat. Phys.* **2006**, *2*, 169.
(2) Khlebnikov S. Preprint at http://arxiv.org/abs/quant-ph/0210019, 2007.
(3) Khlebnikov, S. *Phys. Rev. B* **2008**, *78*, 014512.
(4) (a) McCumber, D. E. *J. Appl. Phys.* **1968**, *39*, 3113. (b) Stewart, W. C. *Appl. Phys. Lett.* **1968**, *12*, 277.
(5) Divochiy, A.; Marsili, F.; Bitauld, D.; Gaggero, A.; Leoni, R.; Mattioli, F.; Korneev, A.; Seleznev, V.; Kaurova, N.; Minaeva, O.; Gol'tsman, G.; Lagoudakis, K. G.; Benkhaoul, M.; Levi, F.; Fiore, A. *Nat. Photon.* **2008**, *2*, 302.
(6) (a) Leggett, A. J. *J. Phys. (Paris)* **1978**, *39*, C6–1264. (b) Caldeira, A. O.; Legget, A. J. *Phys. Rev. Lett.* **1981**, *46*, 211.
(7) Giordano, N. *Phys. Rev. Lett.* **1988**, *61*, 2137.
(8) Lau, C. N.; Markovic, N.; Bockrath, M.; Bezryadin, A.; Tinkham, M. *Phys. Rev. Lett.* **2001**, *87*, 217003.
(9) Altomare, F.; Chang, A. M.; Melloch, M. R.; Hong, Y.; Tu, C. W. *Phys. Rev. Lett.* **2006**, *97*, 017001.
(10) Zgirski, M.; Riikonen, K.-P.; Touboltsev, V.; Arutyunov, K. Yu. *Phys. Rev. B* **2008**, *77*, 054508.
(11) Likharev, K. K. *Rev. Mod. Phys.* **1979**, *51*, 101, and references therein.
(12) Golubov, A. A.; Kupriyanov, M.; Yu.; Il'ichev, E. *Rev. Mod. Phys.* **2004**, *76*, 411, and references therein.
(13) Khlebnikov, S., private communication.
(14) Sellier, H.; Baraduc, C.; Lefloch, F.; Calemczuk, R. *Phys. Rev. Lett.* **2004**, *92*, 257005.
(15) Shapiro, S. J. *Phys. Rev. Lett.* **1963**, *11*, 80.
(16) Anderson, P. W.; Dayem, A. H. *Phys. Rev. Lett.* **1964**, 13–195.
(17) Meidan, D.; Oreg, Y.; Refael, G. *Phys. Rev. Lett.* **2007**, *98*, 187001.
(18) Khlebnikov, S. *Phys. Rev. B* **2008**, *77*, 014505.
(19) Bezryadin, A; Dekker, C. *J. Vac. Sci. Technol. B* **1997**, *15*, 793.
(20) Little, W. A. *Phys. Rev.* **1967**, *156*, 396.
(21) Langer, J. S.; Ambegaokar, V. *Phys. Rev.* **1967**, *164*, 498.
(22) McCumber, D. E.; Halperin, B. I. *Phys. Rev. B* **1970**, *1*, 1054.
(23) Bezryadin, A. *J. Phys.: Condens. Matter* **2008**, *20*, 043202.
(24) Langer−Ambegaokar and McCumber−Halperin (LAMH)[21,22] expressions were used traditionally to fit this curves. Yet, it was pointed out that the LAMH does not apply below $0.9T_C$.[17] Therefore, we simply use the Arrhenius factor with R_N as a prefactor, i.e., the Arrhenius−Little (AL) fit.
(25) Tinkham, M.; Lau, C. N. *App. Phys. Lett.* **2002**, *80*, 2946.
(26) The coherence length at zero temperature $\xi(0)$ is given by $0.855(l\xi_0)^{1/2}$ in the dirty limit, where l is the electric mean free path, ξ_0 [$= \hbar v_F/\pi\Delta$] and Δ [$= 1.76k_BT_C$] are the BCS coherence length and the BCS superconducting gap energy, respectively.
(27) Steinberg, K.; Pressel, M. *Phys. Rev. B* **2008**, *77*, 214517.
(28) (a) Golubev, D.; Zaikin, A. *Phys. Rev. B* **2001**, *64*, 014504. (b) Zaikin, A.; Golubev, D.; Otterlo, A.; Zimanyi, G. T. *Phys. Rev. Lett.* **1997**, *78*, 1552.
(29) (a) Zgirski, M.; Riikonen, K.-P.; Touboltsev, V.; Arutyunov, K. *Nano Lett.* **2005**, *5*, 1029. (b) Zgirski, M.; Riikonen, K.-P.; Holmqvist, T.; Savolainen, M.; Touboltsev, V.; Arutyunov, K. *Quantum Computing in Solid State Systems*; Springer: New York, 2006; Chapter 9.
(30) (a) Bollinger, A. T; Rogachev, A.; Remeika, M.; Bezryadin, A. *Phys. Rev. B* **2004**, *69*, 180503(R). (b) Zgirski, M.; Arutyunov, K. Yu. *Phys. Rev. B* **2007**, *75*, 172509.
(31) (a) Gor'kov, L. P. *J. Exptl. Theoret. Phys. (U.S.S.R.)* **1958**, *34*, 735. (b) Josephson, B. D. *Phys. Lett.* **1962**, *1*, 251.
(32) Troeman, A. G.; Ploeg, S. H. W.; Il'Ichev, E.; Meyer, H.-G.; Golubov, A. A.; Kupriyanov, M. Yu.; Hilgenkamp, H. *Phys. Rev. B* **2008**, *77*, 024509.
(33) Dinsmore, R. C.; Bae, M.-H.; Bezryadin, A. *Appl. Phys. Lett.* **2008**, *93*, 192505.
(34) Kulik, I. O.; Omelyanchuk, A. N. *Pis'ma Zh. Eksp. Teor. Fiz.* **1975**, *21*, 216. [*JETP Lett.* **1975**, *21*, 96].
(35) Likharev, K. K.; Yakobson, L. A. *Zh. Tekhn. Fiz* **1975**, *45*, 1503. [*Sov. Phys. Tech. Phys.* **1975**, *20,* 950].
(36) A scaling factor, b, for the power with the relation of $I_{RF} = \beta P_r^{1/2}$ and I_C are used as the two adjustable parameters.

NL803894M